Eur. Radiol. 10, 1342–1350 (2000)

European
Radiology

Original article

Diffusion-weighted echo-planar MR imaging in differential diagnosis of brain tumors and tumor-like conditions

K. Okamoto[1], **J. Ito**[2], **K. Ishikawa**[1], **K. Sakai**[1], **S. Tokiguchi**[2]

[1] Department of Radiology, Niigata University School of Medicine, 1–757 Asahimachi-dori, Niigata, 951–8510 Japan
[2] Department of Radiology, Niigata University School of Dentistry, 2–5274 Gakkocho-dori, Niigata, 951–8514 Japan

Received: 30 July 1999; Revised: 2 November 1999; Accepted: 9 December 1999

Abstract. We assess diffusion-weighted MR images in the differential diagnosis of intracranial brain tumors and tumor-like conditions. Heavily diffusion-weighted ($b = 1100$ or 1200 s/mm^2) axial images were obtained with single-shot echo-planar technique in 93 patients with pathologically confirmed various intracranial tumors and tumor-like conditions with diffusion gradient perpendicular to the images. We compared signal intensity of the lesions with those of gray and white matter, and cerebrospinal fluid (CSF). In 29 cases (31.1 %) the lesions were isointense to gray and/or white matter. However, 5 cases (5.4 %) showed extremely increased signal intensity: two epidermoid cysts; two chordomas; and one brain abscess. The entire portion of a tumor was markedly hyperintense in 10 cases (10.8 %): four malignant lymphomas; four medulloblastomas; one germinoma; and one pineoblastoma. A CSF-like hypointense signal was seen in many cystic tumors, and cystic or necrotic portions of tumors. A neurosarcoid granulation was the only solid lesion showing characteristically a hypointense signal like CSF. The combination of markedly hyperintense and hypointense signals was seen generally in hemorrhagic tumors. Diffusion-weighted echo-planar MR imaging is useful in the differential diagnosis of brain tumors and tumor-like conditions, and suggests specific histological diagnosis in some cases.

Key words: Brain – MRI – Neoplasms – Diffusion image – Echo-planar MRI

Introduction

Diffusion-weighted MRI can provide us unique information on the diffusion of water molecules, which cannot be obtained with conventional MRI. Its ability to depict fresh cerebral infarction in the acute stage within 6 h of symptom onset is one of the most important clinical aspects [1]. If the diffusion-encoding gradients are comparatively weak, the contrast in the apparent diffusion coefficient (ADC) images will depend on susceptibility, perfusion, and restricted diffusion, but as the strength of the diffusion-encoding gradients becomes greater, the contrast becomes dependent primarily on diffusion [2, 3]. Although diffusion-weighted MR images with strong diffusion gradients have even the possibility of T2 shine through, the images can give us additional information on tissue characterization [2, 4, 5, 6, 7, 8, 9]. However, clinical application of diffusion-weighted MR imaging has been limited, as diffusion-weighted spin-echo (SE) imaging is prone to artifacts from gross motion of the subject as well as pulsation and respiratory motion, which result in image degradation [6, 7, 10, 11].

Recently, diffusion-weighted MR images can be obtained in a few seconds with echo-planar technique and have become more clinically available. However, evaluation of diffusion-weighted MR imaging in the differential diagnosis of brain tumors has been restricted to only a few investigations, to our knowledge [6, 7, 12]. We evaluated the usefulness of echo-planar diffusion-weighted MR images in the differential diagnosis of intracranial brain tumors and tumor-like conditions.

Materials and methods

We studied heavily diffusion-weighted images of 93 patients (51 men and 42 women) with brain tumors (90 cases) or tumor-like conditions (3 cases). Patients' age ranged from 2 months to 77 years (mean age 43.0 years). The diagnosis of the lesions was confirmed pathologically in 85 cases. In the remaining 8 patients with metastatic brain tumors, pathological diagnosis of the primary lesion was confirmed (Table 1).

Heavily diffusion-weighted echo-planar imaging was obtained with a 1.5-T MR unit (Magnetom Vision, Sie-

Correspondence to: K. Okamoto

Table 1. Diagnosis of lesions

		Type 1	Type 2	Type 3	Type 4	Type 5	Type 6	Type 7	Type 8
Brain tumors (n = 90)									
Gliomas	27								
Astrocytic tumors	25								
Glioblastomas	8			1	2	5			
Anaplastic astrocytomas	7			3		2			2
Astrocytomas	5					1		1	3
Pilocystic astrocytomas	4				1			1	2
Xanthoastrocytoma	1							1	
Ependymoma	1					1			
Ganglioma	1					1			
Medulloblastomas	4		4						
Malignant lymphomas	4		4						
Germ cell tumors	4								
Germinoma	2		1		1				
Mixed germ cell tumors	2			2					
Pineocytomas	2								2
Pineoblastoma	1		1						
Hemangioblastoma	1								1
Schwannomas	13			1			1	5	6
Meningiomas	12								
Meningiothelial	9					2			7
Fibroblastic	3					2			1
Chordomas	4	2							2
Rathke cleft cysts	2						2		
Arachnoid cysts	3						3		
Epidermoid cysts	2	2							
Dermoid cyst	1								1
Metastatic brain tumors	10								
Malignant fibrous histiocytoma	1							1[a]	
Breast carcinomas	2					1[a]		1	
Lung carcinomas	2								
Small cell carcinoma	1				1				
Adenocarcinoma	1								1
Malignant melanomas	2				1				1
Esophageal carcinoma	1					1			
Renal cell carcinoma	1				1				
Leukemia	1			1					
Tumor-like conditions (n = 3)									
Brain abscesses	1	1							
Sarcoidosis	1						1		
Langerhans' cell histiocytosis	1					1			
Total	93 (100)	5 (5.4)	10 (10.8)	8 (8.6)	7 (7.5)	17 (18.3)	7 (7.5)	10 (10.8)	29 (31.1)

Numbers in parentheses are percentages
Type 1: Lesions with extremely hyperintense signal (much more hyperintense than the middle cerebellar peduncle or splenium)
Type 2: Lesions with markedly hyperintense signal (iso- or slightly hyperintense to the middle cerebellar peduncle or splenium)
Type 3: Lesions with heterogeneously and markely hyperintense areas in an isointense tumor matrix to gray and white matter
Type 4: Lesions with heterogeneously hyperintense and hypointense signals to gray and white matter
Type 5: Lesions with partially and slightly hyperintense signal to gray and white matter
Type 6: Lesions with markedly hypointense signal like cerebrospinal fluid
Type 7: Lesions with hypointense signal to gray and white matter without hyperintense signal
Type 8: Lesions with isointense signal to gray and for white matter
[a]Metastatic tumour is also pathologically diagnosed

mens, Erlangen, Germany). Axial images were acquired with single-shot echo-planar spin-echo (SE) pulse sequence with following parameters: echo time = 128 ms, field of view = 230 mm, slice thickness = 6 mm, slice gap = 1 mm, a matrix of 128×200, b-value of 1100 or 1200 s/mm^2. Axial pre- and postcontrast T1-weighted SE (TR/TE: 460/12 ms; 2 excitations), T2-weighted turbo-SE (TR/TE: 3000/102 ms; 2 excitations) images, and FLAIR images (TR/TE/TI: 9000/119/2200 ms; 1 excitation) were also obtained with the same slice thickness and interslice gap. When additional thinner slice diffusion-weighted images were obtained, SE or turbo-SE images with the same slice thickness and interslice gap were also acquired. The majority of sellar and suprasellar lesions were excluded from the study except for large tumors with marked suprasellar and third ventricular extension, because susceptibility artifacts obscured lesions on diffusion-weighted images.

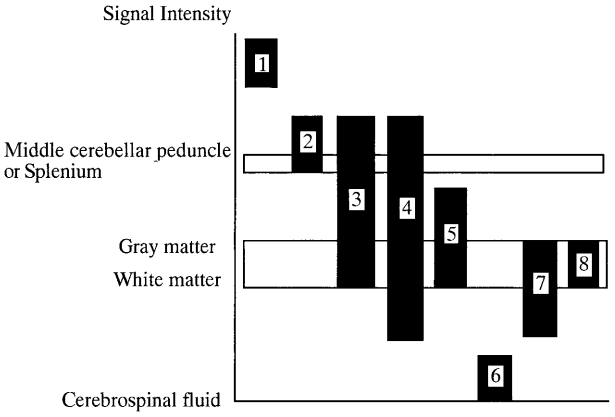

Fig. 1. Signal intensity distribution of each type of the lesions (types 1–8). A *box* indicates signal intensity distribution of the lesion or an anatomical structure. *Number in the black box* indicates the type number

We compared signal intensity of the lesions visually with those of gray and white matter, the middle cerebellar peduncle or splenium of the corpus callosum, and cerebrospinal fluid (CSF) in the ventricles on the same slice of diffusion-weighted images. Relative signal intensity of lesions measured with a region-of-interest (ROI) method was compared with values obtained from normal gray and white matter when necessary.

Lesions were categorized into eight types according to their signal intensity on diffusion-weighted images (Fig. 1). Type 1: lesions with extremely hyperintense signal (much more hyperintense than the middle cerebellar peduncle or splenium of the corpus callosum); type 2: lesions with markedly hyperintense signal (iso- or slightly hyperintense to the middle cerebellar peduncle or splenium of the corpus callosum); type 3: lesions with heterogeneously and markedly hyperintense areas in an isointense tumor matrix to gray and white matter; type 4: lesions with heterogeneously mixed hyperintense and hypointense signals to gray and white matter; type 5: lesions with partially and slightly hyperintense signals to gray and white matter; type 6: lesions with a markedly hypointense signal like CSF; type 7: lesions with a hypointense signal to gray and white matter without hyperintense signal; type 8: lesions with an isointense signal to gray and/or white matter.

Results

Eight signal intensity patterns of lesions on diffusion-weighted images are summarized in Table 1.

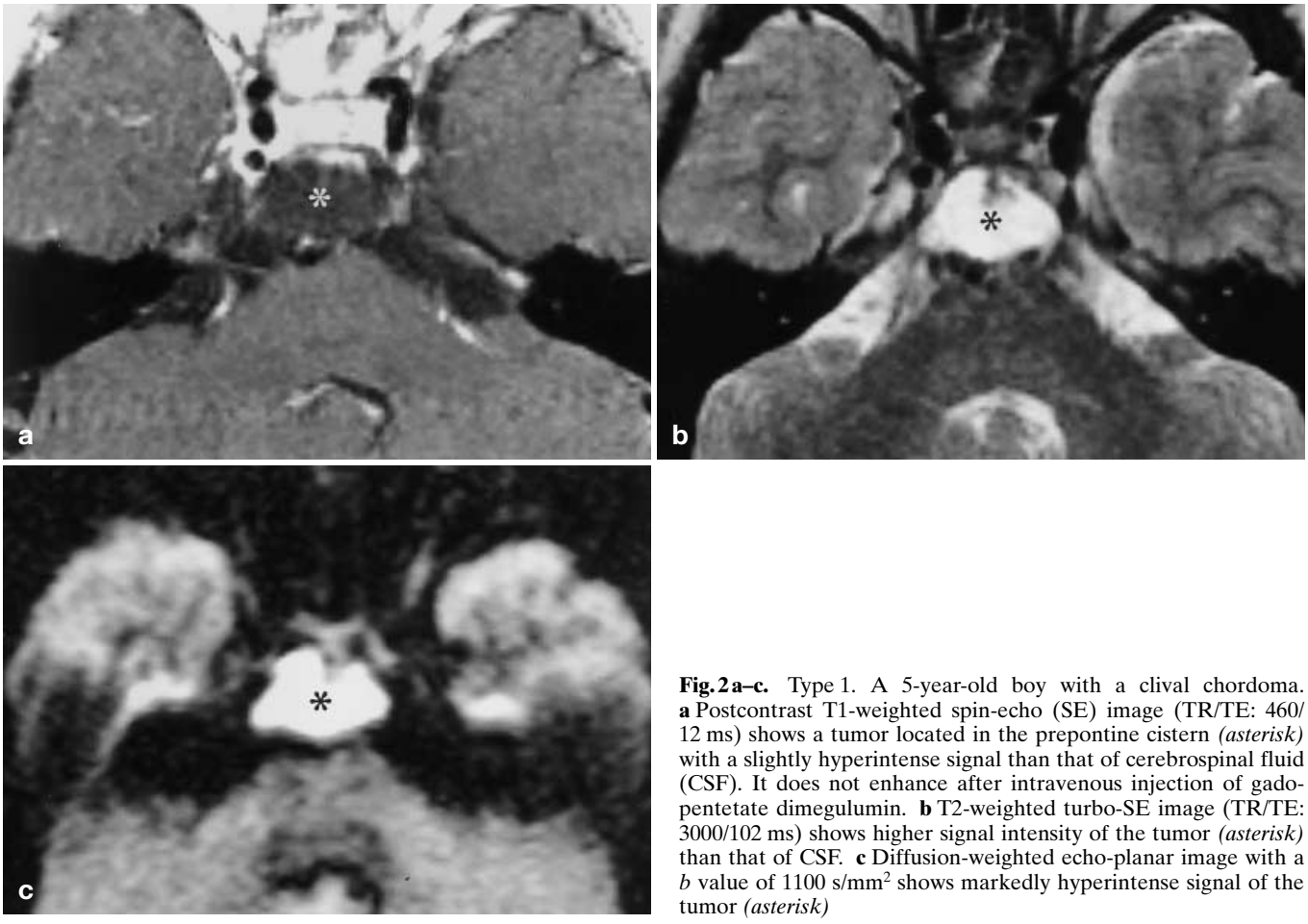

Fig. 2 a–c. Type 1. A 5-year-old boy with a clival chordoma. **a** Postcontrast T1-weighted spin-echo (SE) image (TR/TE: 460/12 ms) shows a tumor located in the prepontine cistern *(asterisk)* with a slightly hyperintense signal than that of cerebrospinal fluid (CSF). It does not enhance after intravenous injection of gadopentetate dimegulumin. **b** T2-weighted turbo-SE image (TR/TE: 3000/102 ms) shows higher signal intensity of the tumor *(asterisk)* than that of CSF. **c** Diffusion-weighted echo-planar image with a *b* value of 1100 s/mm^2 shows markedly hyperintense signal of the tumor *(asterisk)*

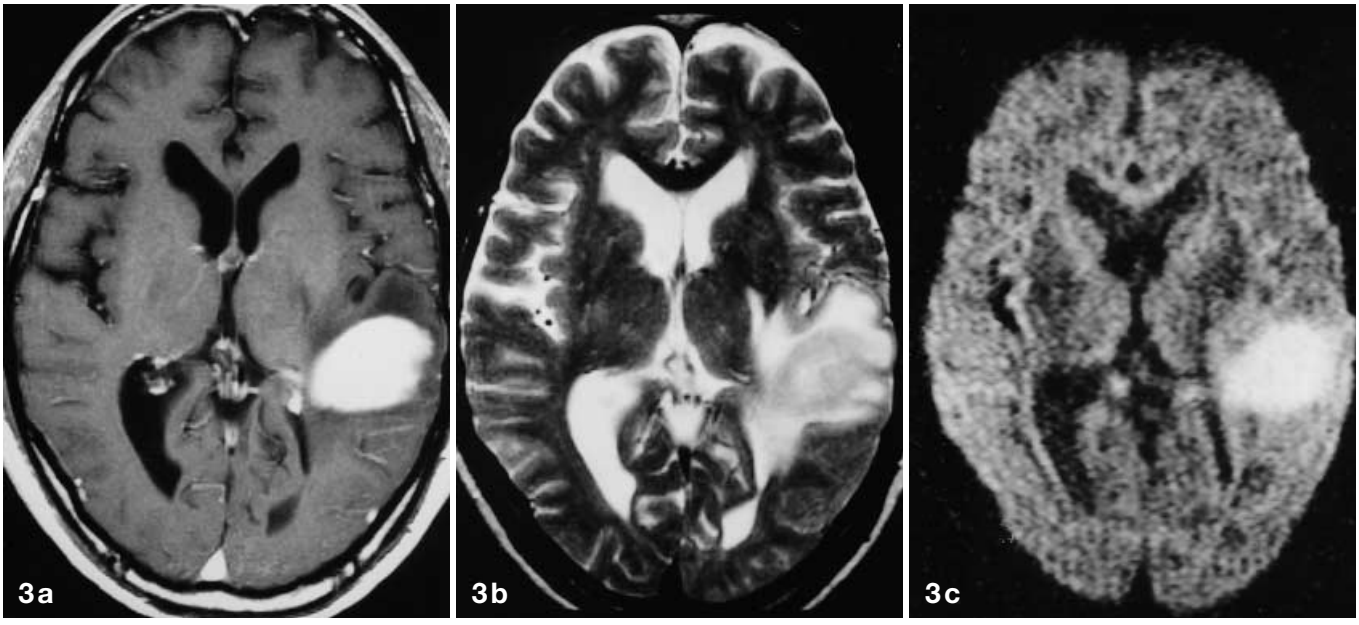

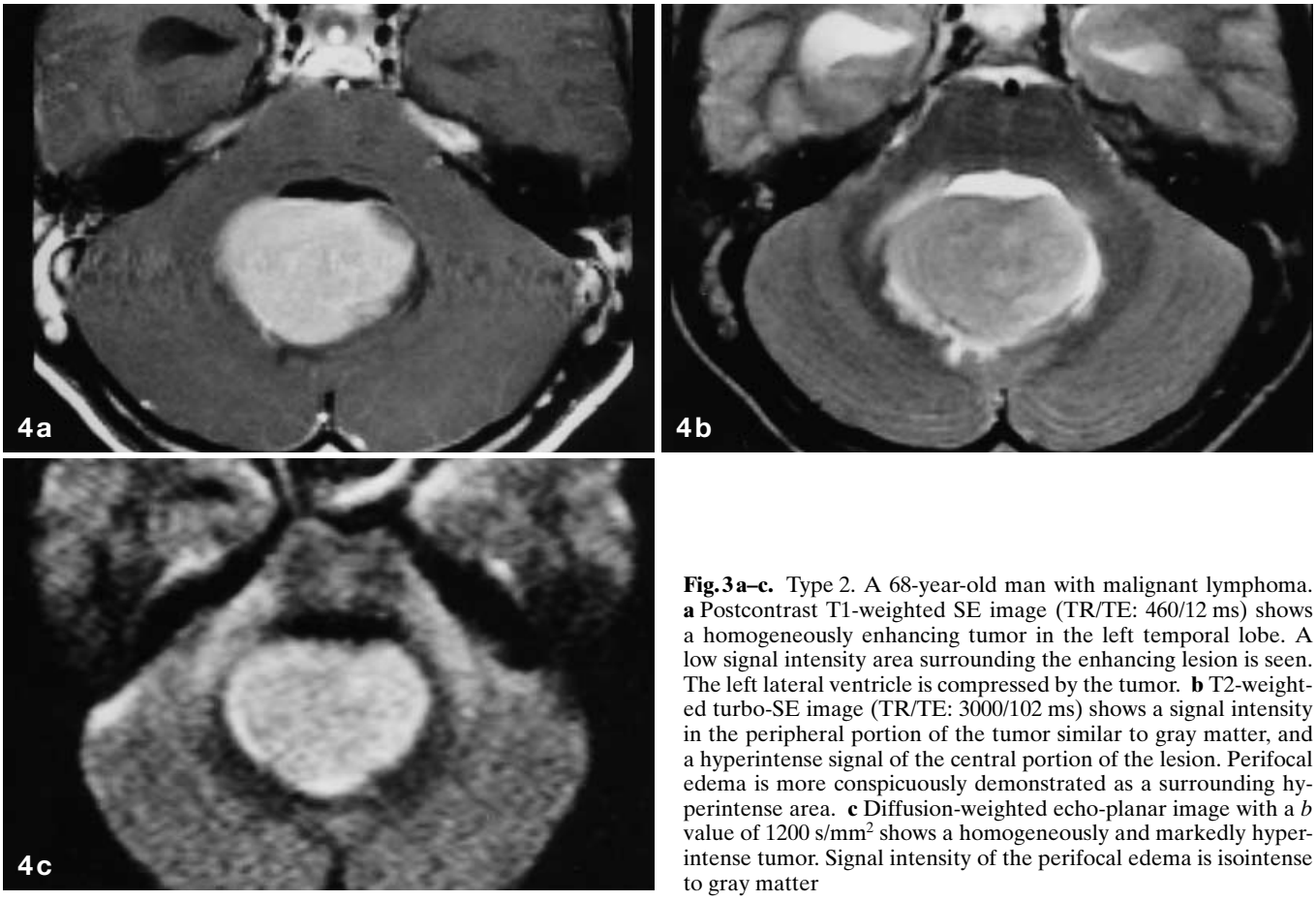

Fig. 3 a–c. Type 2. A 68-year-old man with malignant lymphoma. **a** Postcontrast T1-weighted SE image (TR/TE: 460/12 ms) shows a homogeneously enhancing tumor in the left temporal lobe. A low signal intensity area surrounding the enhancing lesion is seen. The left lateral ventricle is compressed by the tumor. **b** T2-weighted turbo-SE image (TR/TE: 3000/102 ms) shows a signal intensity in the peripheral portion of the tumor similar to gray matter, and a hyperintense signal of the central portion of the lesion. Perifocal edema is more conspicuously demonstrated as a surrounding hyperintense area. **c** Diffusion-weighted echo-planar image with a *b* value of 1200 s/mm^2 shows a homogeneously and markedly hyperintense tumor. Signal intensity of the perifocal edema is isointense to gray matter

Fig. 4 a–c. Type 2. A 22-year-old man with medulloblastoma. **a** Postcontrast T1-weighted SE image (TR/TE: 460/12 ms) shows a homogeneously and markedly enhancing tumor in the dilated fourth ventricle. **b** T2-weighted turbo-SE image (TR/TE: 3000/102 ms) shows slightly higher signal intensity of the tumor than that of cerebellar gray matter. **c** Diffusion-weighted echo-planar imaging with a *b* value of 1200 s/mm^2 shows homogeneously and markedly increased signal intensity of the tumor, which is similar to that of the middle cerebellar peduncles

Type 1 comprised five lesions (5.4 %) including two epidermoid cysts, two chordomas (Fig. 2), and one brain abscess. In four of the five lesions, almost the entire portion of the lesion was extremely hyperintense in signal. One chordoma showed an extremely hyperintense signal in most part of the tumor with heterogeneously hyperintense and hypointense areas that corresponded to intratumoral hemorrhage.

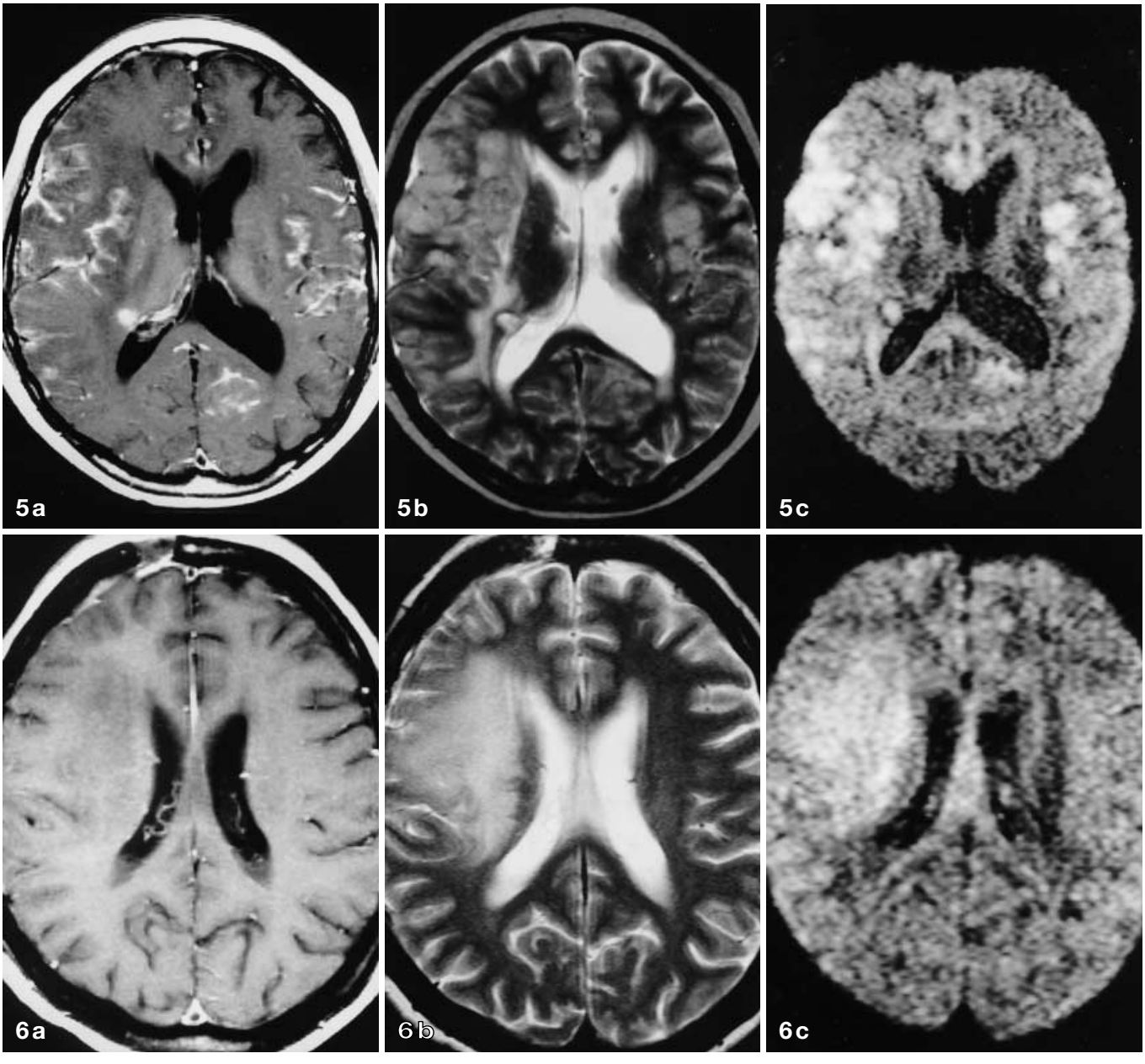

Fig. 5a–c. Type 2. A 16-year-old boy with disseminated medulloblastoma. **a** Postcontrast T1-weighted SE image (TR/TE: 460/12 ms) shows disseminated lesions at the right frontal surface, in the cerebral sulci, and in the bilateral sylvian fissures. **b** Disseminated lesions are seen as hyperintense areas, but each lesion is not so clearly distinguished from the surrounding cerebrospinal fluid and the cerebral cortex on T2-weighted turbo-SE image (TR/TE: 3000/102 ms). **c** Diffusion-weighted echo-planar imaging with a *b* value of 1200 s/mm^2 shows these lesions more conspicuously as markedly hyperintense areas

Fig. 6a–c. Type 3. A 50-year-old woman with anaplastic astrocytoma. **a** Postcontrast T1-weighted SE image (TR/TE: 460/12 ms) shows a slightly hypointense lesion in the right frontal white matter. No enhancing lesion is seen. The right lateral ventricle is smaller than the left. Right frontal cortical sulci are narrower than the left ones. **b** T2-weighted turbo-SE image (TR/TE: 3000/102 ms) shows an ill-defined hyperintense lesion more clearly in the right frontal white matter than on the T1-weighted image **(a)**. **c** Diffusion-weighted echo-planar imaging with a *b* value of 1100 s/mm^2 shows hyperintense signal of the lesion compared with gray matter

Type 2 comprised 10 tumors (10.8%) including four malignant lymphomas (Fig. 3), four medulloblastomas (Fig. 4), one pineoblastoma, and one germinoma. Disseminated lesions of germinoma and medulloblastoma were also demonstrated conspicuously as markedly hyperintense areas on diffusion-weighted images (Fig. 5).

Type 3 comprised eight tumors (8.6%). An irregularly hyperintense area was observed in the peripheral portion of two gliomas (one glioblastoma and one anaplastic astrocytoma). In these gliomas this hyperintense area was shown to spread into the optic radiation and splenium of the corpus callosum. A markedly hyperintense area was seen centrally in two anaplastic gliomas (Fig. 6), two mixed germ cell tumors, and one leukemic involvement of the cerebrum. A vestibular schwannoma with multiple cystic portions showed marked hyperintensity in a central cyst on diffusion-weighted images.

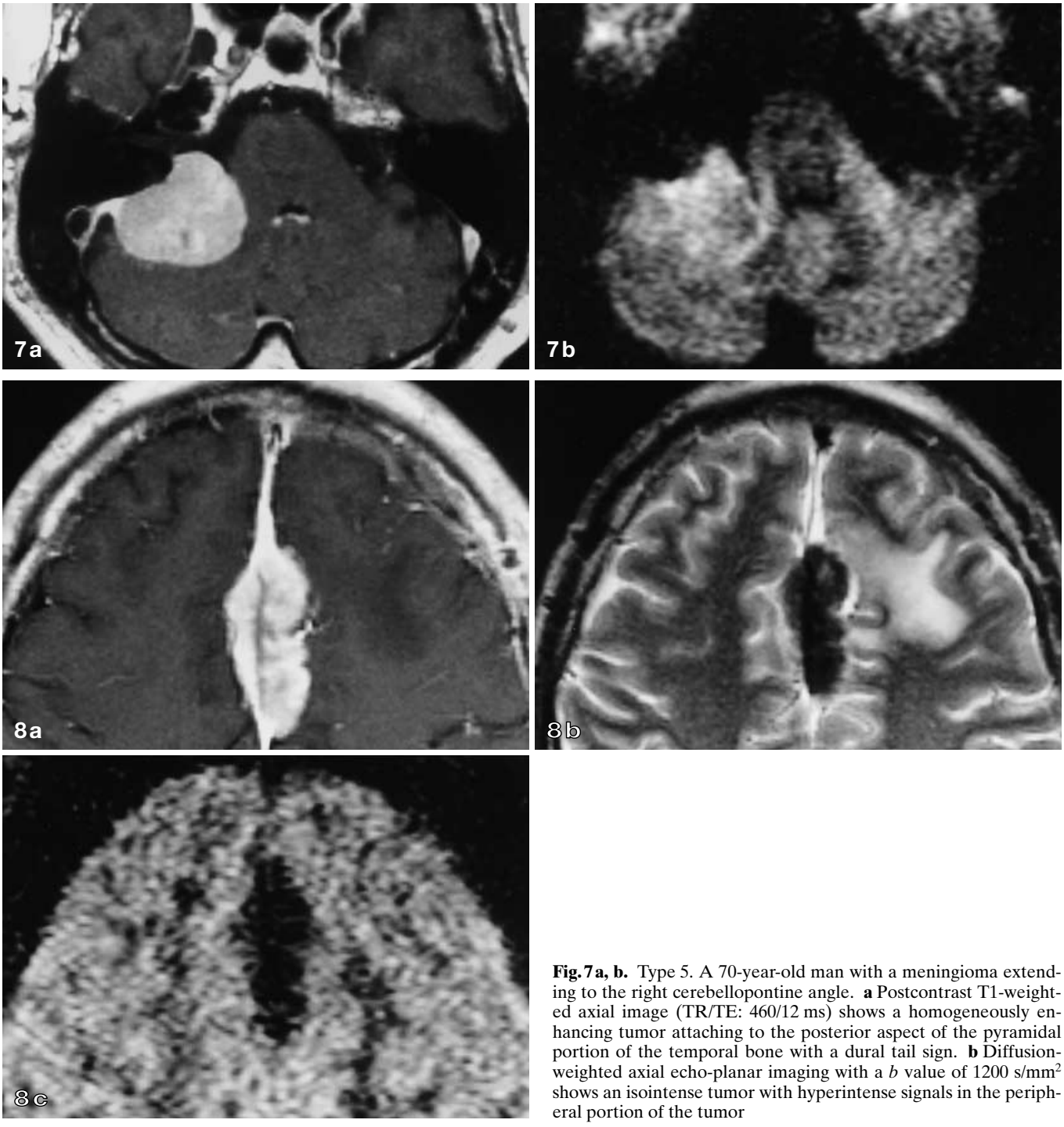

Fig. 7 a, b. Type 5. A 70-year-old man with a meningioma extending to the right cerebellopontine angle. **a** Postcontrast T1-weighted axial image (TR/TE: 460/12 ms) shows a homogeneously enhancing tumor attaching to the posterior aspect of the pyramidal portion of the temporal bone with a dural tail sign. **b** Diffusion-weighted axial echo-planar imaging with a *b* value of 1200 s/mm^2 shows an isointense tumor with hyperintense signals in the peripheral portion of the tumor

Fig. 8 a–c. Type 6. A 28-year-old man with sarcoid granulation of the anterior falx. **a** Postcontrast T1-weighted SE axial image (TR/TE: 460/12 ms) shows an enhancing lesion of the thickened anterior falx. A hypointense area is seen in the left frontal white matter and is considered as accompanying edema. **b** T2-weighted turbo-SE axial image (TR/TE: 3000/102 ms) shows a markedly hypointense signal of the lesion, which is lower than that of white matter. The left frontal white matter lesion is hyperintense to gray matter. **c** Diffusion-weighted axial echo-planar imaging with a *b* value of 1200 s/mm^2 shows markedly hypointense signal of the lesion. Signal intensity of the left frontal white matter lesion is isointense to gray matter

Type 4 comprised seven tumors (7.5 %). Six of these lesions had intratumoral hemorrhage. In a germinoma in the third ventricle, a solid part of the lesion was markedly hyperintense, but multiple intratumoral cysts were markedly hypointense.

Type 5 comprised 17 lesions (18.3 %). Both gadolinium-enhanced portion and non-enhanced necrotic portions in gliomas, metastatic tumors, and a Langerhans cell histiocytosis corresponded to the hyperintense areas on diffusion-weighted images. In meningiomas, increased signal intensity was seen in the periphery (Fig. 7).

Type 6 comprised seven tumors (7.5%); six were cystic tumors. Also included in this category was one sarcoid lesion mimicking an en plaque meningioma of the anterior falx (Fig. 8). This lesion was entirely solid.

Type 7 comprised 10 tumors (10.8%). Nine lesions had relatively large intratumoral cysts with isointense small solid portions. However, a metastatic malignant fibrous histiocytoma showed a large hypointense central area on diffusion-weighted images without intratumoral hemorrhage or a corresponding large cystic portion (Fig. 9).

Type 8 consisted of the remaining 29 tumors (31.1%). This group included various intra- and extra-axial tumors (Fig. 10). Margins of tumors in this category could not be well defined, or even the presence of a tumor was unclear on diffusion-weighted images.

Discussion

Diffusion-weighted images with strong diffusion gradients are independent of spin density, T1, or T2, but are dependent on the diffusion of water molecules in the section studied [4]. It can give us additional information on tissue characterization, which could not be obtained with conventional MRI. Normal gray matter with a relatively packed and organized cellular structure restricts movement of the water molecule, and it does not show directional restriction of diffusion, and is termed isotropic [4]. However, restriction of the water molecule can also be observed in normal white matter tracts, i.e., water is relatively unrestricted along white matter tracts but is restricted orthogonal to white matter tracts, which is termed anisotropy. White matter oriented in the direction of the diffusion gradient has an elevated ADC, whereas white matter orthogonal to the direction of the diffusion gradient has a markedly decreased ADC [4]. The ADC in gray matter is lower than in white matter parallel to the direction of diffusion gradient, and is higher than in white matter orthogonal to the direction [4]. As structures with a lower ADC appear to be more hyperintense on diffusion-weighted images, normal white matter tracts orthogonal to the direction of the diffusion gradient along the cephalocaudal axis, such as the middle cerebellar peduncle, splenium of the corpus callosum, and superior longitudinal fasciculus, are hyperintense to gray matter on diffusion-weighted axial images. White matter tracts parallel to the direction of the diffusion gradient including the internal capsule and corona radiata are markedly hypointense. Other portions of cerebral white matter is slightly hypointense to gray matter on heavily diffusion-weighted images.

In our study, approximately one third of various intra- and extra-axial tumors had isointense signal to gray and/or white matter on diffusion-weighted images. The ADC in contrast-enhancing gliomas is reported to be within the range of that of normal cerebral white or gray matter [7]. The ADC in meningiomas does not differ significantly from that seen in high-grade gliomas or cerebral metastases [7, 12]. However, some brain tumors and tumor-like conditions showed characteristically altered signal intensities on diffusion-weighted images. Epidermoid cysts and brain abscess showed the mostly increased signal intensity in our study. This observation is in agreement with previous reports [3, 6]. In addition, two of four chordomas had a hyperintense signal, which might have resulted from abundant mucinous matrix of chordomas. However, chordomas may show various signal intensities, or a heterogeneous signal in the same tumor, because cytoarchitecture varies widely, and calcification and hemorrhage may be present [13]. Epidermoid cysts and chordomas are both extra-axial tumors. Brain abscess was the sole intra-axial lesion showing a characteristically hyperintense signal on diffusion-weighted images in our study. A brain abscess could be differentiated from other intra-axial tumors, such as gliomas or metastatic brain tumors, showing similar ring-like enhancement on gadolinium-enhanced images [14, 15].

In a total of 10 cases of malignant lymphoma, medulloblastoma, germinoma, and pineoblastoma, almost the entire portion of the tumor showed a homogeneous and markedly hyperintense signal. It is interesting that these tumors are composed of densely packed cells with large nuclei and scanty cytoplasm. Disseminated lesions of medulloblastoma and germinoma were more conspicuously depicted on diffusion-weighted images than on any other imaging sequences, including gadolinium-enhanced images, even if they were very small, i.e., measuring less than 5 mm in diameter.

Marked and more heterogeneous hyperintensities were seen in various hemorrhagic intra-axial tumors including gliomas and metastatic tumors. However, these lesions were usually accompanied by hypointense signals. The combination of these markedly high- and low signal intensities on diffusion-weighted images may suggest intratumoral hemorrhage, but not histological typing of tumors.

Leukemic lesions and high-grade gliomas without intratumoral hemorrhage demonstrated a markedly hyperintense signal in the tumor matrix partially or heterogeneously. Tien et al. reported that gadolinium-enhanced portion is hyperintense on diffusion-weighted images in high-grade gliomas [4]. However, a non-enhanced portion of six high-grade gliomas showed hyperintense signal in our study (Fig. 6). In general, a hyperintense signal was usually seen in high-grade gliomas (glioblastomas, 8 of 8 = 100%; anaplastic astrocytomas, 5 of 7 = 71.4%), and many low-grade gliomas were isointense or hypointense to gray matter on diffusion-weighted images (astrocytoma, 4 of 5 = 80%; pilocytic astrocytomas, 3 of 4 = 75.0%; xanthoastrocytoma, 1 of 1 = 100%). Although a slightly hyperintense signal could be seen in low-grade gliomas (astrocytomas 1 of 5 = 20%, ependymoma 1 of 1 = 100%, ganglioglioma 1 of 1 = 100%), a markedly hyperintense signal was seen in only high-grade gliomas except for one case of pilocytic astrocytoma with intratumoral hemorrhage. Sugahara et al. reported that low-grade gliomas exhibited iso- to mild hyperintensity compared with the gray matter on the diffusion-weighted images, and glioblastomas exhibited hyperintensity compared with the gray matter.

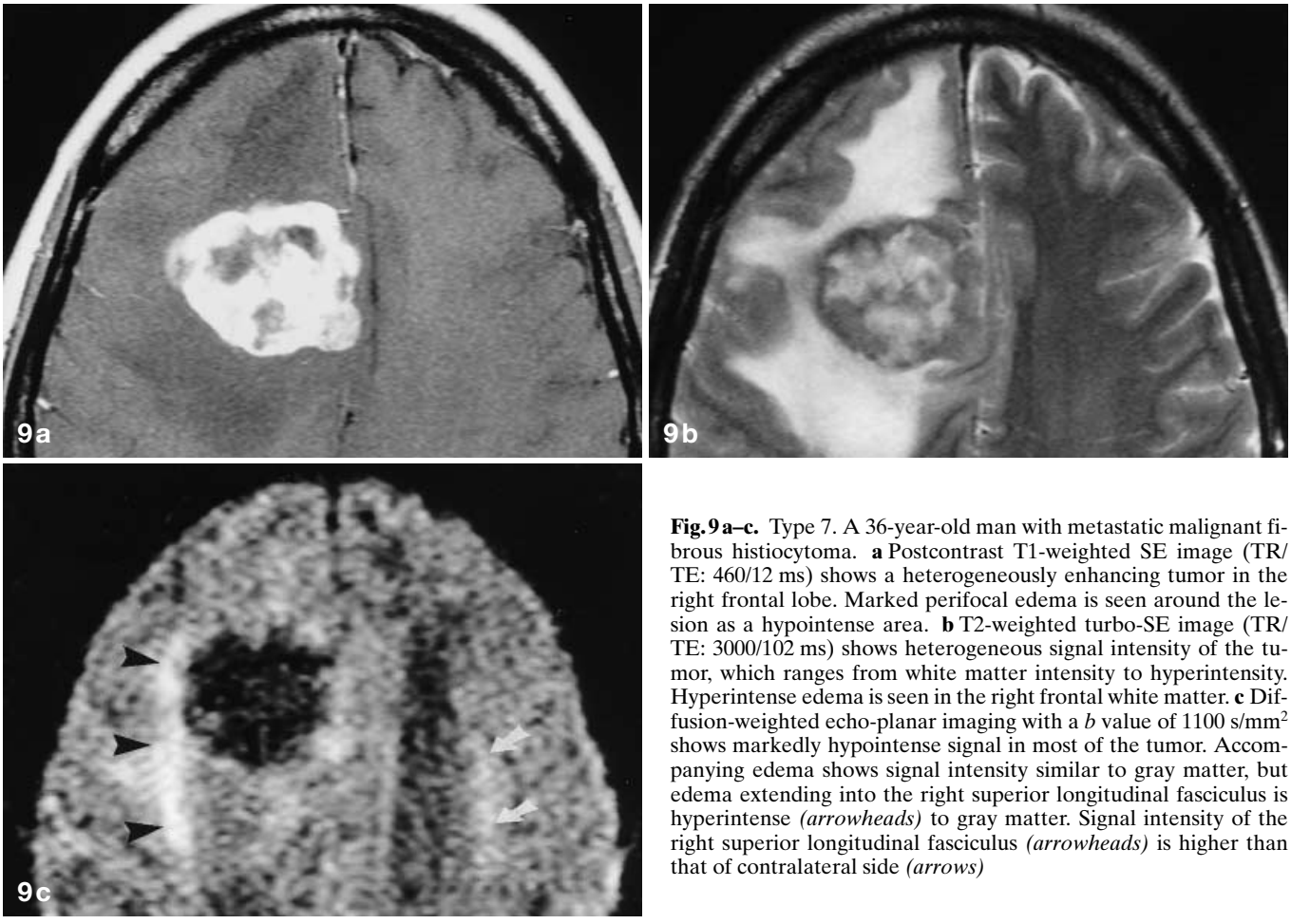

Fig. 9 a–c. Type 7. A 36-year-old man with metastatic malignant fibrous histiocytoma. **a** Postcontrast T1-weighted SE image (TR/TE: 460/12 ms) shows a heterogeneously enhancing tumor in the right frontal lobe. Marked perifocal edema is seen around the lesion as a hypointense area. **b** T2-weighted turbo-SE image (TR/TE: 3000/102 ms) shows heterogeneous signal intensity of the tumor, which ranges from white matter intensity to hyperintensity. Hyperintense edema is seen in the right frontal white matter. **c** Diffusion-weighted echo-planar imaging with a *b* value of 1100 s/mm^2 shows markedly hypointense signal in most of the tumor. Accompanying edema shows signal intensity similar to gray matter, but edema extending into the right superior longitudinal fasciculus is hyperintense *(arrowheads)* to gray matter. Signal intensity of the right superior longitudinal fasciculus *(arrowheads)* is higher than that of contralateral side *(arrows)*

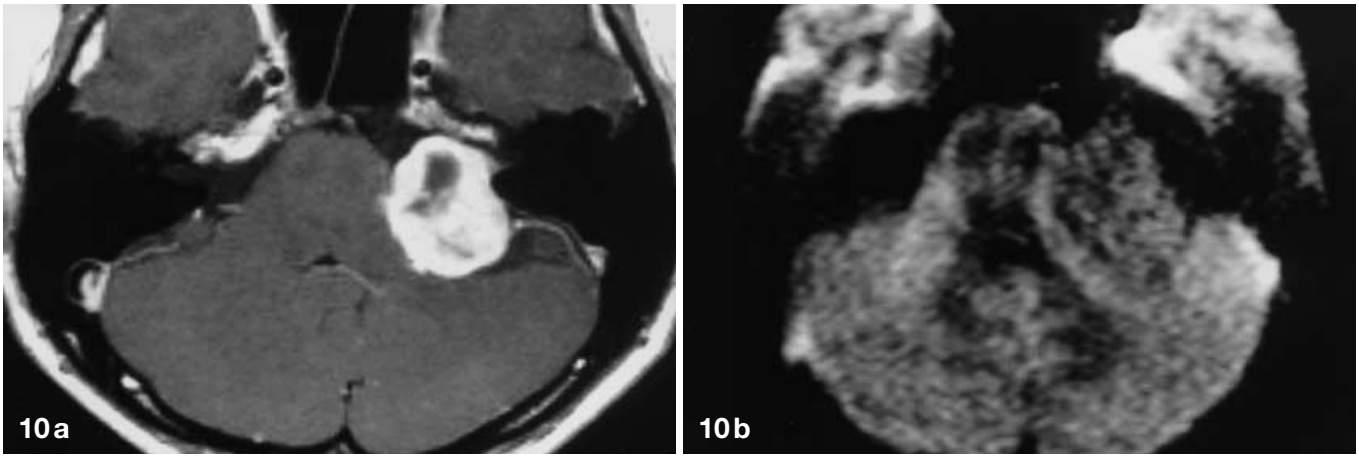

Fig. 10 a, b. Type 8. A 38-year-old woman with a vestibular schwannoma at the left cerebellopontine angle. **a** Postcontrast T1-weighted image (TR/TE: 460/12 ms) shows an enhancing tumor with small cystic portions in the tumor matrix. **b** The tumor is isointense on a diffusion-weighted image with a *b* value of 1100 s/mm^2

The minimum ADC value of the gliomas correlates well with tumor cellularities [16]. In addition to gliomas, some meningiomas as well as metastatic brain tumors could show slightly hyperintense signal on diffusion-weighted images (type 5).

A greater degree of signal suppression is seen when non-enhancing gliomas infiltrate white matter tracts that run parallel to the direction of the diffusion gradient [4]. On the other hand, tumor invasion or perifocal edema extending into the white matter tracts orthogonal to the diffusion gradient, including the optic radiation, splenium of the corpus callosum, or superior longitudinal fasciculus, caused marked increase in signal intensity of these structures on diffusion-weighted images (Fig. 9c); these might result from additional increase of anisotropy in white matter.

In meningiomas a slightly hyperintense signal was seen peripherally. Although the compressed middle cerebellar peduncle by neurinomas showed increased signal intensity on diffusion-weighted images, neurinomas themselves did not show peripheral hyperintense signals (Fig. 10). If peripheral hyperintensity on diffusion-weighted images is seen in an extra-axial tumor, meningioma is more likely than neurinoma. The increased signal of the compressed middle cerebral peduncle should not be confused with peripheral hyperintensity of the tumor itself. The mechanisms of this hyperintense signal in meningiomas are not yet clear. The difference in cytoarchitecture between meningiomas and neurinomas might be one of the mechanisms.

In addition to cystic tumors, such as arachnoid cysts and large Rathke cleft cysts, most necrotic portions of gliomas or metastatic tumors, or cystic portions of neurinomas, showed a markedly hypointense signal like that of CSF in the ventricle on diffusion-weighted images. Our observation is compatible with previous reports [4, 6, 7].

Sarcoid lesions presenting as dural-based disease may be indistinguishable from meningiomas or lymphomatous disease on MR imaging [17]. However, our case of sarcoidosis involving the anterior falx was of markedly hypointense signal, which was not demonstrated in any other solid neoplastic lesions including meningiomas or lymphomas. This characteristic hypointensity might differentiate a granulomatous disease from neoplastic lesions.

Metastatic malignant fibrous histiocytoma showed a large central hypointense area on diffusion-weighted images without hyperintense signal. On MR images with other pulse sequences, this tumor had no large cystic or necrotic portion corresponding to the hypointense area on diffusion-weighted images. The tumor consisted mainly of fibroblast-like neoplastic cells and a considerable amount of collagen fibrils histologically. Plump spindle cells arranged in short fascicles in a cartwheel or storiform pattern might be a cause of the hypointensity on diffusion-weighted images.

Our experience is limited and further examinations are needed to evaluate the usefulness of the diffusion-weighted images in the differential diagnosis of brain tumors and tumor-like conditions. Diffusion-weighted images have the possibility of T2 shine through, and ADC map images without effect of T2 shine through can be made at multiple *b*-values. The ADC map images are more suitable for accurate evaluation of ADC of the lesion. In addition, diffusion tensor imaging can provide more precise information on the amount and directional bias (anisotropy) of diffusion in lesions [18]. However, diffusion-weighted images with strong diffusion gradients give us useful information on tissue characterization, and show histological nature of the brain tumor or tumor-like conditions. A histological diagnosis is suggested in some cases. The images can be acquired in a few seconds with the echo-planar technique; therefore, diffusion-weighted images should be added in routine MR imaging of patients suspected of having a brain tumor or tumor-like condition.

References

1. González RG, Schaefer PW, Buonanno FS, Schwamm LH, Budzik RF, Rofdorf G, Wang B, Sorensen AG, Koroshetz WJ (1999) Diffusion-weighted MR imaging: diagnostic accuracy in patients imaged within 6 hours of stroke symptom onset. Radiology 210: 155–162
2. Le Bihan D, Breton E, Lallemand D, Aubin ML, Vignaud J, Lavel-Jeantet M (1988) Separation of diffusion and perfusion in intravoxel incoherent motion MR imaging. Radiology 168: 497–505
3. Henkelman RM (1990) Diffusion-weighted MR imaging: a useful adjunct to clinical diagnosis or a scientific curiosity? Am J Neuroradiol 11: 932–934
4. Tien RD, Felsberg GJ, Friedman H, Brown M, MacFall J (1994) MR imaging of high-grade cerebral gliomas: value of diffusion-weighted echoplanar pulse sequences. Am J Roentgenol 162: 671–677
5. Le Bihan D, Breton E, Lallemand D, Grenier P, Cabanis E, Laval-Jeantet M (1986) MR imaging of intravoxel incoherent motions: application to diffusion and perfusion in neurologic disorders. Radiology 161: 401–407
6. Tsuruda JS, Chew WM, Moseley ME, Norman D (1990) Diffusion-weighted MR imaging of the brain: value of differentiating between extraaxial cysts and epidermoid tumors. Am J Neuroradiol 11: 925–931
7. Krabbe K, Gideon P, Wagn P, Hansen U, Thomsen C, Madsen F (1997) MR diffusion imaging of human intracranial tumours. Neuroradiology 39: 483–489
8. Chien D, Buxton RB, Kwong KK, Brady TJ, Rosen BR (1990) MR diffusion imaging of the human brain. J Comput Assist Tomogr 14: 514–520
9. Hajnal JV, Doran M, Hall AS, Collins AG, Oatridge A, Pennock JM, Young IR, Bydder GM (1991) MR imaging of anisotropically restricted diffusion of water in the nervous system: technical, anatomic, and pathologic considerations. J Comput Assist Tomogr 15: 1–18
10. Le Bihan D (1988) Intravoxel incoherent motion imaging using steady-state free precession. Magn Reson Med 7: 346–351
11. Chenevert TL, Pipe JG (1991) Effect of bulk tissue motion on quantitative perfusion and diffusion magnetic resonance imaging. Magn Reson Med 19: 261–265
12. Yanaka K, Shirai S, Kimura H, Kamezaki T, Matsumura A, Nose T (1995) Clinical application of diffusion-weighted magnetic resonance imaging to intracranial disorders. Neurol Med Chir (Tokyo) 35: 648–654
13. Lantos PL, VandenBerg SR, Kleihues P (1997) Chordomas. In: Graham DI, Lantos PL (eds) Greenfield's neuropathology, 6th edn. Arnold, London, pp 776–780
14. Ebisu T, Tanaka C, Umeda M, Kitamura M, Naruse S, Higuchi T, Ueda S, Sato H (1996) Discrimination of brain abscess from necrotic or cystic tumors by diffusion-weighted echo planar imaging. Magn Reson Imaging 14: 1113–1116
15. Tuchiya K, Yamakami N, Hachiya J, Saito I, Kobayashi H (1998) Multiple brain abscesses, differentiation from cerebral metastases by diffusion-weighted magnetic resonance imaging. Int J Neuroradiol 4: 258–262
16. Sugahara T, Korogi Y, Kochi M, Ikushima I, Shigematu Y, Hirai T, Okuda T, Liang L, Ge Y, Komohara Y, Ushio Y, Takahasi M (1999) Usefulness of diffusion-weighted MRI with echo-planar technique in the evaluation of cellularity in gliomas. J Magn Reson Imaging 9: 53–60
17. Goldberg HI, Lavi E, Atlas SW (1996) Sarcoidosis. In: Atlas SW (ed) Magnetic resonance imaging of the brain and spine, 2nd edn. Lippincott-Raven, Philadelphia, pp 448–449
18. Werring DJ, Clark CA, Barker GJ, Thmpson AJ, Miller DH (1999) Diffusion tensor imaging of lesions and normal-appearing white matter in multiple sclerosis. Neurology 52: 1626–1632